

Random number generation with a chaotic electromechanical resonator

Guilhem Madiot

Centre de Nanosciences et de Nanotechnologies, CNRS, Université Paris-Saclay,
91120 Palaiseau, France

Franck Correia

Centre de Nanosciences et de Nanotechnologies, CNRS, Université Paris-Saclay,
91120 Palaiseau, France

Sylvain Barbay

Centre de Nanosciences et de Nanotechnologies, CNRS, Université Paris-Saclay,
91120 Palaiseau, France

Remy Braive

Centre de Nanosciences et de Nanotechnologies, CNRS, Université Paris-Saclay,
Palaiseau, France

Université de Paris, F-75006 Paris, France

Institut Universitaire de France, Paris, France

E-mail: remy.braive@c2n.upsaclay.fr

Abstract. Chaos enables the emergence of randomness in deterministic physical systems. Therefore it can be exploited for the conception of true random number generators (RNG) mandatory in classical cryptography applications. Meanwhile, nanomechanical oscillators, at the core of many on-board functionalities such as sensing, reveal as excellent candidates to behave chaotically. This is made possible thanks to intrinsic mechanical nonlinearities emerging at the nanoscale. Here we present a platform gathering a nanomechanical oscillator and its integrated capacitive actuation. Using a modulation of the resonant force induced by the electrodes, we demonstrate chaotic dynamics and study how it depends on the dissipation of the system. The randomness of a binary sequence generated from a chaotic time trace is evaluated and discussed such that the generic parameters enabling successful random number generation can be established. This demonstration makes use of concepts which are sufficiently general to be applied to the next generation of nano-electro-optomechanical systems.

1. Introduction

The combination of integrated electronics and suspended micro or nanomechanics in micro-nano electromechanical systems (M&NEMS) have led to a large number of industrial applications that have now invaded our daily lives such as, e.g., accelerometers or gyroscopes [1], all present in a modern smartphone. M&NEMS are also likely to be used as gas, mass or pressure sensors, and have also potential for biomedical applications [2]. Although these devices generally rely on the static response of a mechanical component to an external stimulus, e.g. the acceleration provoked by a car accident in an air-bag trigger, it can also be interesting to exploit the resonance phenomena occurring in these mechanical structures. By coupling the latter with an excitation scheme, such as a piezoelectric or capacitive actuator, one can resonantly drive the mechanical motion. This configuration finds an immediate application with microphone which convert electrical signals to acoustic waves, and reciprocally. By reducing the dimensions of these electromechanical systems at the nanoscale, one can not only access the radio-frequency (RF) domain, but also unavoidably allow nonlinear phenomena to manifest in the dynamics of these devices. Interestingly such nonlinear behavior is not necessarily a drawback but can actually be exploited. Amplification of weak signals, for example, can be achieved using NEMS thanks to a bistable regime enabled by a structural Duffing anharmonicity of the material [3, 4].

Among the possible regimes achievable with such nonlinear oscillators, chaos might be the most intriguing as it enables the introduction of unpredictability in classical and deterministic physical systems. Thus chaos emerges as a possible solution to generate true randomness without appealing to stochastic [5] or quantum [6] phenomena. In this spirit there have been several proposals to generate true random number sequences out of a chaotic time trace [7, 8, 9, 10, 11]. Several approaches using mechanical systems have also been considered [12, 13, 14], for pseudo-RNG applied to image encryption [15], and applied with bit-rate above 100 MHz [16], but rely on an external chaotic generator.

Here we present an integrated electromechanical device based on photonic-crystal (PhC) membrane and interdigitated electrodes (IDE) separated by a nanometric air-gap (see [figs. 1a](#) and [1b](#)). Such a system enables controlled chaos to emerge using a slowly-modulated electromechanical force [17, 18, 19]. An in-depth study of chaotic dynamics is performed upon the mechanical dissipation. Applying a threshold to generate random binary sequences from chaotic time traces, we evaluate the randomness quality as a function of two parameters involved in the sequence

generation. Importantly, this study goes way beyond the scope of our system and could be applied to any system displaying similar driven chaotic dynamics [18].

Our experiment, which gathers both electromechanical actuation and optical readout aided by a integrated optical cavity, enables the transduction of the mechanical motion into the optical domain. This ability to gather electromechanical and optical properties within the same device constitutes the basis for the development of nano-opto-electro-mechanical systems (NOEMS) [20, 21, 22, 23]. The multiplication of such novel platforms respond the interest focused to specific functionalities, such as optical-to-RF conversion [24, 25, 26], or opto-electro-mechanical switches [27, 28], for example.

2. System description and Nanofabrication

To gather the mechanical, electrical and optical properties into such NOEMS, we base the design on a 260 nm thick suspended InP membrane. This $20 \times 10 \mu\text{m}^2$ rectangular membrane constitutes a mechanical resonator whose quality factor can be significantly increased by optimizing the four bridges connecting the membrane to the substrate [29]. Electromechanical actuation is enabled by the integration of IDE below the free-standing membrane. The latter is engineered as an optical reflector by etching it through with a 2D photonic crystal which maximizes its normal reflexion coefficient [30].

The main steps of the nanofabrication process flow are schematically depicted in [fig. 1c](#). They include a) the electron beam lithography (EBL) of the IDE on a silicon wafer, followed by metal deposition and lift off; b) the heterogeneous BCB-bonding [31] on the Si wafer of a InP substrate incorporating the InP membrane onto which 350 nm of SiN is deposited by PECVD and chemical InP substrate removal; c) the EBL patterning of the mechanical structures and photonic crystals followed by ICP etching of the InP layer; and d) Under-etching of the mechanical structure (etching of the SiN layer) with HF, followed by critical point drying. The resulting platform is shown in the colored SEM micrograph in [fig. 1d](#).

The 350 nm air gap separating the membrane from the IDE placed below constitutes an optical cavity at the He-Ne wavelength (633 nm). This optomechanical readout permits to enhance the sensitivity to detect the membrane out-of-plane resonances [32]. Meanwhile the dielectric properties of the membrane makes it easier to be excited by capacitive actuation. Both DC gate V_{dc} and RF signal $V_{\text{ac}} \cos(2\pi f_{\text{d}}t)$ are applied externally between these two electrodes and the field lines penetrate and polarize the InP membrane. In [fig. 1b](#), we show the stationary solution for the electric

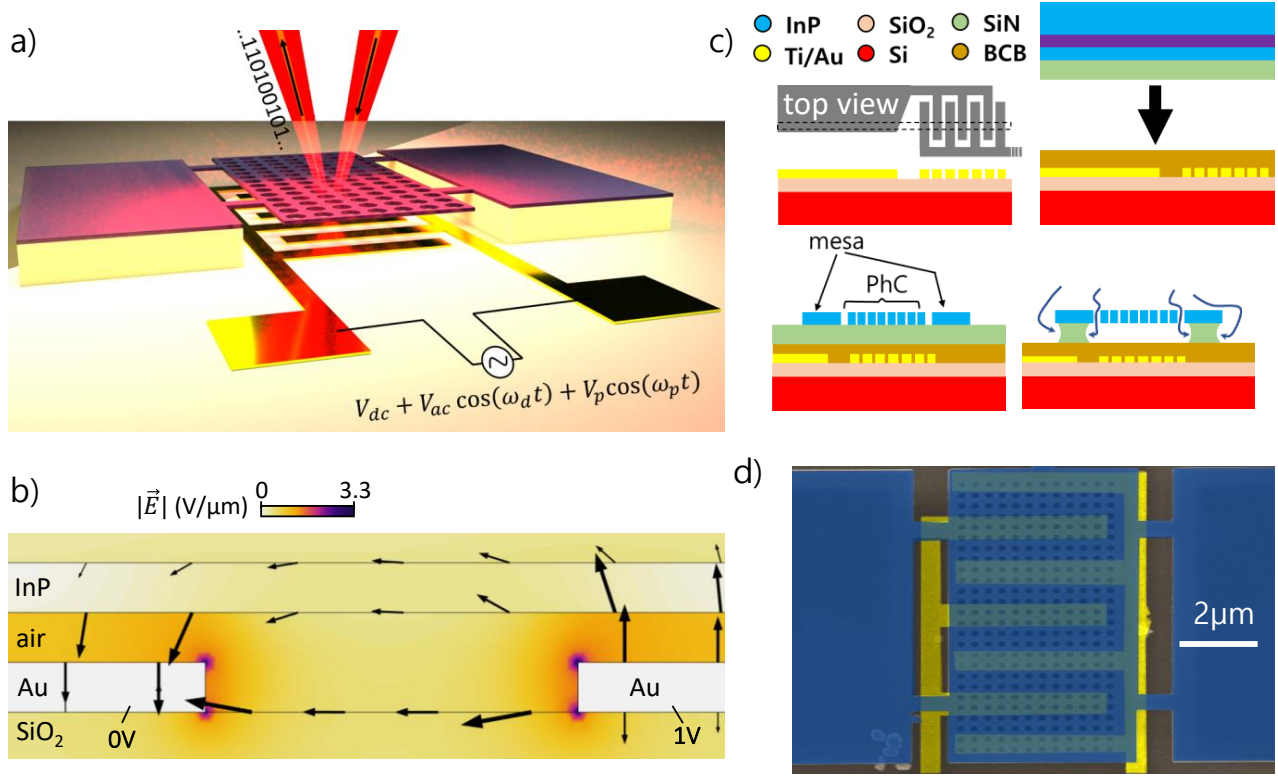


Figure 1: a) Artistic view of the platform and random number generation encrypted in the readout optical field. b) FEM simulation of the electric field in a simplified cross-section of the system. The black arrows show the vector field \vec{E} which its norm is shown in color. c) Fabrication process: IDEs deposition by EBL and lift off, integration of an InP substrate by heterogeneous bonding, EBL definition of the mechanical structures and ICP, under-etching and CPD. d) colorized SIM micrograph with the PhC membrane (blue) and IDT shown in transparency (yellow).

vector field \vec{E} (arrows) and norm $|\vec{E}|$ (colorscale) in the system, obtained by Finite-Element Simulation methods. This model accounts for a 2D cross-section of the structure, with electrical potential of 1V imposed every two gold digit while the others are grounded. This produces electric field arcs that cross the above InP membrane, which induces a capacitive force on it. Experimentally, the oscillating contribution of this force is proportional to $V_{dc}V_{ac} \cos(2\pi f_d t)$. Therefore when the actuation frequency f_d approaches a mechanical resonance f_m , the mechanical oscillation amplitude of the membrane increases. With this system, we are interested in probing the first order mode of the membrane which has the highest overlap with the incident optical field. This "drum" mode has the strongest out-of-plane amplitude and therefore is prone to exhibit nonlinearity, which is essential in the following to obtain a chaotic dynamics.

3. Dissipation parameters control and influence on chaotic dynamics

The sample is placed in a vacuum chamber pumped at 10^{-6} mbar. The He-Ne laser is focused at the center of the membrane. Several mechanical modes are observed between 2 and 15 MHz. As discussed above, we focus on the fundamental mode, with frequency $f_m = 2.327$ MHz. The associated IDE is submitted to a voltage $V_{dc} + V_{ac} \cos(2\pi f_d t)$ with $V_{dc} = 2$ V and $V_{ac} = 0.5$ V. While scanning the driving frequency f_d around the mechanical resonance, we demodulate the photoreceived optical signal with a passband filter centered at f_d and 100 Hz wide, returning both demodulated amplitude V and phase φ . The amplitude voltage can be converted into a mechanical displacement r after calibration.

This measurement is reproduced for different values of the pressure in the vacuum chamber and four representative spectral responses are shown in fig. 2a. We note a significant broadening of the mechanical

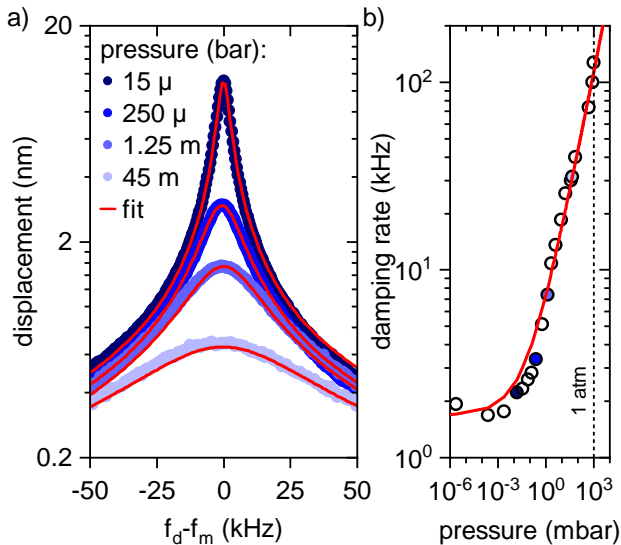


Figure 2: a) Normalized spectral response of the mechanical mode at different pressure condition in the vacuum chamber with Lorentzian fits (red lines). b) Pressure dependence of the mechanical damping (do, with a power-law fit (red line).

resonance while the pressure increases. This results from the increasing contribution of air-damping in the mechanical dissipation. We fit each resonance curve with the Lorentzian lineshape (red lines) and extract the mechanical damping rate. The latter is plotted as a function of the pressure in [fig. 2b](#). An exponential increase is observed above 1 mbar while a saturation to $\gamma_0 \sim 2$ kHz is observed below this value. The saturation arises when the mechanical losses are no longer dominated by air-damping but rather explainable by internal mechanical loss channels such as clamping and thermomechanical losses.

So far we have used sufficiently low input voltages V_{ac} and V_{dc} for the mechanics to remain in the linear regime, where the system can be treated as a driven harmonic oscillator. Increasing the applied electromechanical force leads to nonlinear responses that typically manifest itself by a mechanical bistability. This is experimentally verified by scanning f_d forward and backward around the mechanical frequency. Such measurement is shown in [fig. 3a](#) at three different values of the vacuum chamber pressure. The data are normalized by their respective maximum and the linear lineshape (see [fig. 2a](#)) are reported here for reference. In each case we apply the same excitation with $V_{ac} = 3$ V. We note that a relatively small increase of the mechanical linewidth provokes a significant change in the bistability, whose frequency span tends to reduce.

In the following we induce a chaotic dynamics

by performing an amplitude modulation of the electromechanical force [32, 17, 18, 19]. We add a new RF drive – we refer as the pump signal – $V_p \cos(2\pi f_p t)$ which leads to near-resonant force amplitude $F(t) \propto V_{dc}(V_{ac} + V_p \cos(2\pi f_p t))$. The driving frequency f_d is set at the low-frequency edge of the bistability, ensuring a wider bandwidth for the chaotic regime [17].

Both the pump amplitude V_p and frequency f_p can be played with to tune the dynamical regime of mechanical responses. Increasing the amplitude for a fixed frequency typically leads to a period-doubling cascade route to chaos [32]. Here we rather set the pump amplitude to $V_p = 2.5$ V and scan the frequency from 2 kHz to 20 kHz. The mechanical response time traces $r(t)$ and $\varphi(t)$ are recorded for 100 ms. The quadrature $Y(t) = r(t) \sin(\varphi(t))$ is used to reconstruct a Poincaré section of the signal. The latter is plotted as a function of f_p in the bifurcation diagrams shown in [fig. 3b](#).

At low pressure, the mechanical displacement induces sufficiently strong nonlinearity to enable a driven chaotic dynamics, as illustrated at $P = 15$ μ bar. The cascaded period doubling to chaos is observed for decreasing f_p , and starts around 16.5 kHz. The presence of chaos can be numerically verified by computing the Largest Lyapunov Exponent, that we show in red below this bifurcation diagram. A zero LLE indicates a periodic or quasi periodic motion whereas a strictly positive LLE corresponds to a chaotic dynamics. The presence of experimental noise slightly increases the LLE giving rise to a slightly positive value even for periodic motion but the significant increase at some specific positions – from 6.6 to 14.5 kHz – clearly indicates the range of f_p in which chaos emerges. These regions are also visually identifiable on the diagram as they translate into a dense Poincaré section. Here the chaos spans over ~ 8 kHz but this range tends to reduce when the mode linewidth increases, since this comes also with a decrease of the mechanical nonlinearity, the bistability span being strongly dependent on the damping rate. Thus at 125 μ bar the bifurcation diagram does not display a chaotic regime although a period-doubling is observed at ~ 12 kHz. The dynamics keeps getting poorer as the pressure in the chamber increases, as illustrated with the third panel taken at 250 μ bar.

4. Random number generation

Now that we have described the conditions under which chaos can be reached, we can focus on the exploitation of this dynamical regime to generate random numbers. Here we apply a method enabling the production of a sequence of random bits from an experimental chaotic time trace. This is achieved using a method

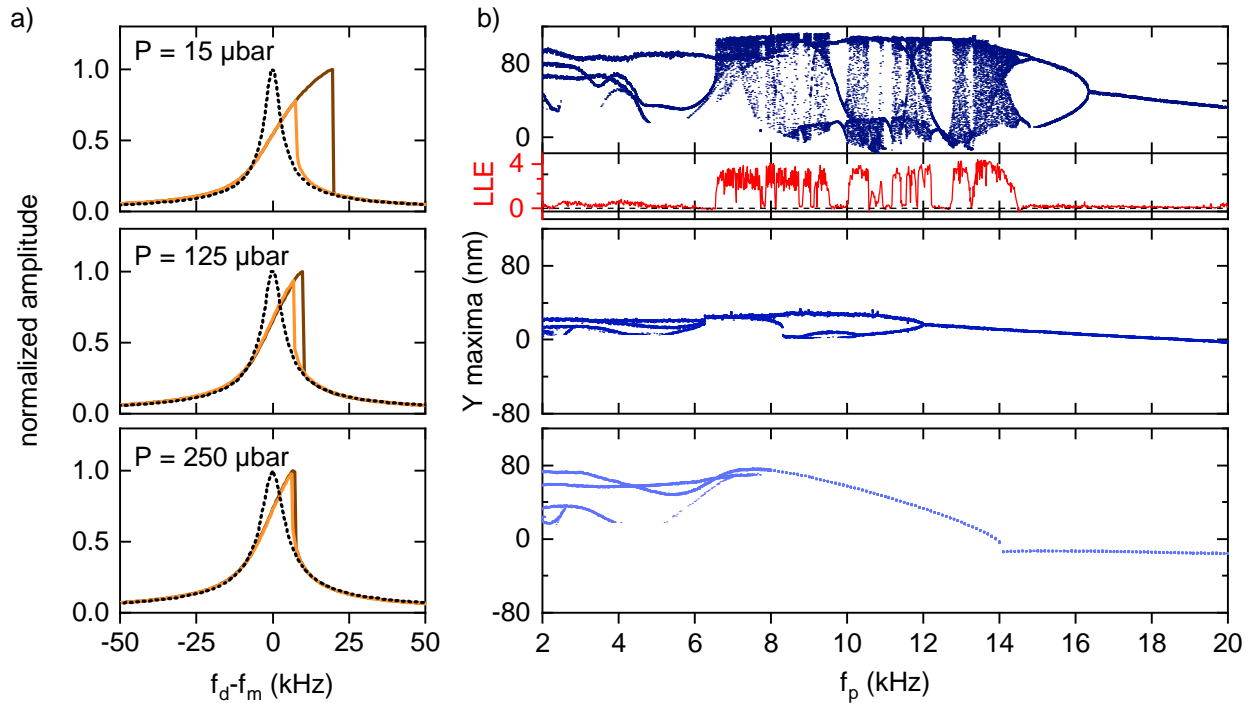


Figure 3: For 3 different values of the pressure in the vacuum chamber : a) Normalized mechanical displacement with forward (brown) and backward (orange) sweep of the driving frequency around mechanical frequency $f_m = 2.327$ MHz. The linear response is indicated for reference (back dashed). b) Experimental bifurcation diagram parametrized with the pump frequency f_p .

described in [33] where the sign of a time trace is periodically compared to a delayed copy of itself with the logical function XOR. We record the quadrature $X(t) = r(t) \cos(\varphi(t))$ for $f_p = 12.3$ kHz and $V_p = 2.5$ V. In practice, we consider the normalized time trace $(X - \langle X \rangle) / \sigma_X$ where $\langle X \rangle$ and σ_X are the mean value and the standard deviation of $X(t)$ calculated over the full time trace, respectively. Note that the following results remain unchanged by using the other quadrature, $Y(t)$. The normalized time trace under study is shown in fig. 4a. We introduce a delay τ and a sampling frequency f_s , which corresponds to the rate at which $X(t)$ and $X(t - \tau)$ will be compared (see fig. 4b). The bits resulting from the XOR gate applied between the respective signs of these two traces are shown in fig. 4c.

In the following the randomness of a binary sequence is verified by applying the NIST Statistical Test Suite [34]. It is composed by 14 randomness tests, each returning a p-value that can be interpreted as the probability for the sequence to be random according to the corresponding test. The p-value validates the test if its value is above 0.01. In the following we simply apply all these algorithms on our binary sequence and check the p-values. If all the p-values validate the sequence as random, we consider that this sequence passes the randomness test. On the contrary, if at least one test

fails, we consider the sequence as not random.

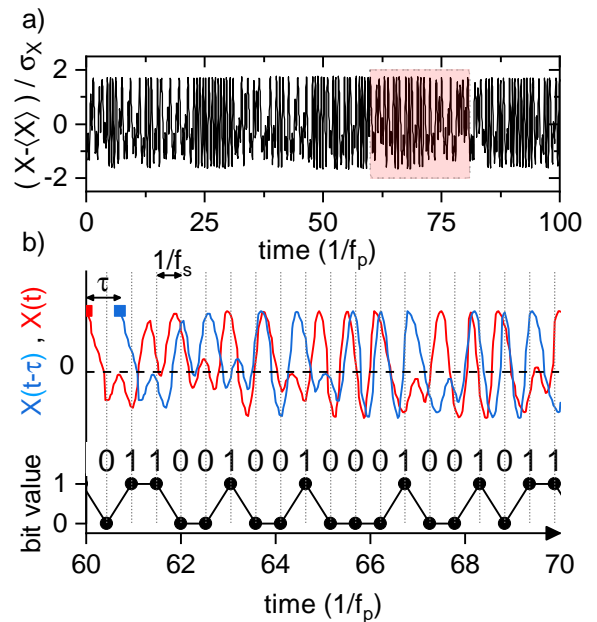


Figure 4: a) Experimental chaotic time trace. b) The trace $X(t)$ is compared to its delayed self $X(t - \tau)$. c) The XOR logical gate is periodically applied to the traces relative sign. It results in a binary sequence.

Our objective is to characterize the randomness test success as a function of the delay τ and the sampling frequency f_s . By generating a binary sequence for several values of τ and f_s , we plot a matrix showing the randomness test result in fig. 5. The green (resp. red) pixels correspond to a successful (resp. unsuccessful) test. Both the sampling frequency and the delay are shown in units of pump frequency and pump period, respectively. f_p^{-1} corresponds to the mean oscillation period of the chaotic trace. We observe a significant increase of the randomness quality towards low sampling frequencies, with a threshold limit around 0.35. This is related to the modulation frequency f_p in the present case. Indeed at high sampling frequencies, the trace does not have enough time to evolve between two samples. This favors the apparition of runs of ones and zeros ('00', '11', '000', '111', and so on) which break the sequence randomness. Moreover the randomness quality shows significant degradation at $f_p\tau = 1$ and 2. This relates with a strong correlation between $X(t)$ and $X(t - \tau)$ for these values of the delay. Overall, low sampling frequency and high delay improve the randomness of the sequence. Randomness can emerge only if τ is sufficiently high for the two trace to decorrelate. Beyond these specific points, fig. 5 evidences many pairs of delay and sampling frequency allowing random number generation.

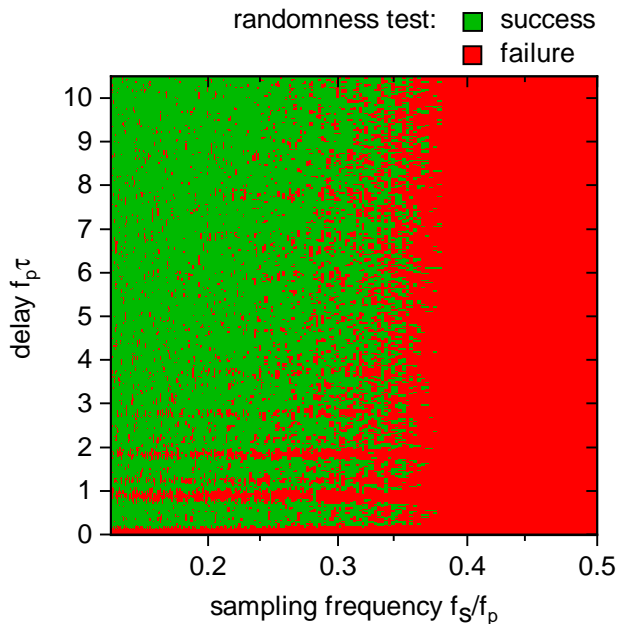


Figure 5: Randomness test suite result as a function of the delay τ and the sampling frequency f_s applied to the trace presented in fig. 4a. Both quantities are shown in units of modulation period.

5. Conclusion

We have presented a nano-electromechanical system displaying driven chaotic dynamics when submitted to a periodically time-varying force. In a first experiment, we submit the mechanical system to different environmental condition, by controlling the pressure in the vacuum chamber. From the dissipative properties of the system, we conclude on their effect on the dynamics of the nonlinear system. The emergence of chaos is clearly favoured by a higher mechanical quality factor, as this comes with a more pronounced bistability.

Using a chaotic time trace to generate binary sequences, we study the randomness of the latter as a function of two control parameter. We draw general conclusions about the respective influence of these two buttons, and relate these dependencies with the physics of the system. RNG in a driven chaotic system such as the one presented here could benefit from the use of two quadratures while only one is considered here. Simultaneous generation of random bits using both quadratures could multiply the bit-rate by two, and even more in multimode systems, if several drives and demodulation channels are used at the same time [32].

In addition, the dynamics under study here is scalable, i.e. it could be reproduced in other types of devices, performing at higher frequencies, and relying of a different physics. The condition for chaos to emerge relies on the presence of an intrinsic nonlinearity triggering bistable behaviours in the system on the one hand, and on the time-modulation of the driving force on the other hand. Therefore, Kerr optical cavities as well as optomechanical system could be exploited to reproduce these results a higher frequency, in which case the subsequent bit-rate could reach several Gbs.

Acknowledgments

This work is supported by the French RENATECH network, the European Union's Horizon 2020 research innovation program under grant agreement No 732894 (FET Proactive HOT), the Agence Nationale de la Recherche as part of the "Investissements d'Avenir" program (Labex NanoSaclay, ANR-10-LABX-0035) with the flagship project MaCaCQu and the JCJC project ADOR (ANR-19-CE24-0011-01).

- [1] Robert Bogue. Mems sensors: past, present and future. *Sensor Review*, 2007.
- [2] Shekhar Bhansali and Abhay Vasudev. *MEMS for biomedical applications*. Elsevier, 2012.
- [3] Avishek Chowdhury, Sylvain Barbay, Marcel G Clerc, Isabelle Robert-Philip, and Rémy Braive. Phase

- Stochastic Resonance in a Forced Nanoelectromechanical Membrane. *Phys. Rev. Lett.*, 119(23):234101, 2017.
- [4] Avishek Chowdhury, Marcel G Clerc, Sylvain Barbay, Isabelle Robert-Philip, and Remy Braive. Weak signal enhancement by nonlinear resonance control in a forced nano-electromechanical resonator. *Nature Communications*, 11(1):2400, 2020.
 - [5] Lishuang Gong, Jianguo Zhang, Haifang Liu, Luxiao Sang, and Yuncai Wang. True random number generators using electrical noise. *IEEE Access*, 7:125796–125805, 2019.
 - [6] Giuseppe Vallone, Davide G. Marangon, Marco Tomasin, and Paolo Villoresi. Quantum randomness certified by the uncertainty principle. *Phys. Rev. A*, 90:052327, Nov 2014.
 - [7] M Sciamanna and K A Shore. Physics and applications of laser diode chaos. *Nature Photonics*, 9:151–162, 2015.
 - [8] Minseo Kim, Unsoo Ha, Kyuho Jason Lee, Yongsu Lee, and Hoi-Jun Yoo. A 82-nw chaotic map true random number generator based on a sub-ranging sar adc. *IEEE Journal of Solid-State Circuits*, 52(7):1953–1965, 2017.
 - [9] Binglei Shi, Ciwei Luo, Jaime G Flor Flores, Guoqiang Lo, Dim-Lee Kwong, Jiagui Wu, and Chee Wei Wong. Gbps physical random bit generation based on the mesoscopic chaos of a silicon photonics crystal microcavity. *Optics Express*, 28(24):36685–36695, 2020.
 - [10] Fei Yu, Lixiang Li, Qiang Tang, Shuo Cai, Yun Song, and Quan Xu. A survey on true random number generators based on chaos. *Discrete Dynamics in Nature and Society*, 2019, 2019.
 - [11] Binglei Shi, Ciwei Luo, Jaime G. Flor Flores, Guoqiang Lo, Dim-Lee Kwong, Jiagui Wu, and Chee Wei Wong. Gbps physical random bit generation based on the mesoscopic chaos of a silicon photonics crystal microcavity. *Opt. Express*, 28(24):36685–36695, Nov 2020.
 - [12] Jonathan Voris, Nitesh Saxena, and Tzipora Halevi. Accelerometers and randomness: Perfect together. In *Proceedings of the Fourth ACM Conference on Wireless Network Security*, WiSec '11, page 115–126, New York, NY, USA, 2011. Association for Computing Machinery.
 - [13] Teh-Lu Liao, Pei-Yen Wan, and Jun-Juh Yan. Design of Synchronized Large-Scale Chaos Random Number Generators and Its Application to Secure Communication. *Applied Sciences*, 9(1), 2019.
 - [14] W. G. Dantas, Lucas R. Rodrigues, Sebastian Ujevic, and Andr  o Gusso. Using nanoresonators with robust chaos as hardware random number generators. *Chaos: An Interdisciplinary Journal of Nonlinear Science*, 30(4):043126, 2020.
 - [15] Serhii Haliuk, Oleh Krulikovskyi, Dmytro Vovchuk, and Fernando Corinto. Memristive structure-based chaotic system for prng. *Symmetry*, 14(1):68, 2022.
 - [16] Miguel Garcia-Bosque, Adri  n P  rez, Carlos S  nchez-Azqueta, and Santiago Celma. Application of a mems-based trng in a chaotic stream cipher. *Sensors*, 17(3), 2017.
 - [17] Martial Defoort, Libor Rufer, Laurent Fesquet, and Skandar Basrour. A dynamical approach to generate chaos in a micromechanical resonator. *Microsystems & nanoengineering*, 7(1):1–11, 2021.
 - [18] Samer Hourri, Motoki Asano, Hiroshi Yamaguchi, Nat-sue Yoshimura, Yasuharu Koike, and Ludovico Minati. Generic rotating-frame-based approach to chaos generation in nonlinear micro- and nanoelectromechanical system resonators. *Phys. Rev. Lett.*, 125:174301, Oct 2020.
 - [19] John Miles. Chaotic motion of a weakly nonlinear, modulated oscillator. *Proceedings of the National Academy of Sciences*, 81(12):3919–3923, 1984.
 - [20]   rko Zobenica, Rob W. van der Heijden, Maurangelo Petruzzella, Francesco Pagliano, Rick Leijssen, Tian Xia, Leonardo Midolo, Michele Cotrufo, YongJin Cho, Frank W. M. van Otten, Ewold Verhagen, and Andrea Fiore. Integrated nano-opto-electro-mechanical sensor for spectrometry and nanometrology. *Nature Communications*, 8(1):2216, Dec 2017.
 - [21] Leonardo Midolo, Albert Schliesser, and Andrea Fiore. Nano-opto-electro-mechanical systems. *Nature Nanotechnology*, 13(1):11–18, 2018.
 - [22] Nan Xu, Ze-Di Cheng, Jin-Dao Tang, Xiao-Min Lv, Tong Li, Meng-Lin Guo, You Wang, Hai-Zhi Song, Qiang Zhou, and Guang-Wei Deng. Recent advances in nano-opto-electro-mechanical systems. *Nanophotonics*, 10(9):2265–2281, 2021.
 - [23] Daniel Navarro-Urrios, Mart  n F. Colombano, Guillermo Arregui, Guilhem Madiot, Alessandro Pitanti, Amadeu Griol, Tapani Makkonen, Jouni Ahopelto, Clivia M. Sotomayor-Torres, and Alejandro Mart  nez. Room-temperature silicon platform for ghz-frequency nanoelectro-opto-mechanical systems. *ACS Photonics*, 9(2):413–419, 2022.
 - [24] Joerg Bochmann, Amit Vainsencher, David D Awschalom, and Andrew N Cleland. Nanomechanical coupling between microwave and optical photons. *Nature Physics*, 9(11):712–716, 2013.
 - [25] T. Bagci, A. Simonsen, S. Schmid, L. G. Villanueva, E. Zeuthen, J. Appel, J. M. Taylor, A. S  rensen, K. Usami, A. Schliesser, and E. S. Polzik. Optical detection of radio waves through a nanomechanical transducer. *Nature*, 507(7490):81–85, Mar 2014.
 - [26] Krishna C Balam, Marcelo I Davan  o, Jin Dong Song, and Kartik Srinivasan. Coherent coupling between radiofrequency, optical and acoustic waves in piezo-optomechanical circuits. *Nature photonics*, 10(5):346–352, 2016.
 - [27] Tianran Liu, Francesco Pagliano, and Andrea Fiore. Nano-opto-electro-mechanical switch based on a four-waveguide directional coupler. *Opt. Express*, 25(9):10166–10176, May 2017.
 - [28] Christian Haffner, Andreas Joerg, Michael Doderer, Felix Mayor, Daniel Chelladurai, Yuriy Fedoryshyn, Cosmin Ioan Roman, Mikael Mazur, Maurizio Burla, Henri J. Lezec, Vladimir A. Aksyuk, and Juerg Leuthold. Nano–opto-electro-mechanical switches operated at cmos-level voltages. *Science*, 366(6467):860–864, 2019.
 - [29] Avishek Chowdhury. *Mechanical nonlinear dynamics of a suspended photonic crystal membrane with integrated actuation*. PhD thesis, Universit   Paris Saclay (COMUE), 2016.
 - [30] Thomas Antoni, Aur  lien G Kuhn, Tristan Briant, Pierre-Fran  ois Cohadon, Antoine Heidmann, R  my Braive, Alexios Beveratos, Izo Abram, Luc Le Gratiet, Isabelle Sagnes, et al. Deformable two-dimensional photonic crystal slab for cavity optomechanics. *Optics letters*, 36(17):3434–3436, 2011.
 - [31] T. J. Karle, Y. Halioua, F. Raineri, P. Monnier, R. Braive, L. Le Gratiet, G. Beaudoin, I. Sagnes, G. Roelkens, F. van Laere, D. Van Thourhout, and R. Raj. Heterogeneous integration and precise alignment of in-paved photonic crystal lasers to complementary metal-oxide semiconductor fabricated silicon-on-insulator wire waveguides. *Journal of Applied Physics*, 107(6):063103, 2010.
 - [32] Guilhem Madiot, Franck Correia, Sylvain Barbay, and R  my Braive. Bichromatic synchronized chaos in driven coupled electro-optomechanical nanoresonators. *Phys. Rev. A*, 104:023525, Aug 2021.
 - [33] Kunihito Hirano, Taiki Yamazaki, Shinichiro Morikatsu, Haruka Okumura, Hiroki Aida, Atsushi Uchida, Shigeru Yoshimori, Kazuyuki Yoshimura, Takahisa Harayama,

and Peter Davis. Fast random bit generation with bandwidth-enhanced chaos in semiconductor lasers. *Opt. Express*, 18(6):5512–5524, Mar 2010.

- [34] Lawrence E Bassham, Andrew L Rukhin, Juan Soto, James R Nechvatal, Miles E Smid, Elaine B Barker, Stefan D Leigh, Mark Levenson, Mark Vangel, David L Banks, Nathanael Alan Heckert, James F Dray, and San Vo. SP 800-22 Rev. 1a. A Statistical Test Suite for Random and Pseudorandom Number Generators for Cryptographic Applications. Technical report, NIST, Gaithersburg, MD, USA, 2010.